Available online at www.sciencedirect.com

SciVerse ScienceDirect

Ceramics International 38 (2012) 5879–5887

CERAMICS INTERNATIONAL

www.elsevier.com/locate/ceramint

Grain size effect on the structural and dielectric properties of $Pb_{0.85}La_{0.15}TiO_3$ ferroelectric ceramic compound

Alexandre Mesquita [a,b], Maria Inês Basso Bernardi [a], Claude Godart [b], Paulo Sergio Pizani [c], Alain Michalowicz [b], Valmor Roberto Mastelaro [a,*]

[a] Instituto de Física de São Carlos (IFSC), Universidade de São Paulo, São Carlos, SP, Brazil
[b] Institut de Chimie et des Materiaux Paris Est, CNRS and Université Paris Est, 94320 Thiais, France
[c] Departamento de Física, Universidade Federal de São Carlos, São Carlos, SP, Brazil

Received 18 February 2012; received in revised form 11 April 2012; accepted 12 April 2012
Available online 11 May 2012

Abstract

This paper presents a study of the influence of particle size on the structural and dielectric properties of $Pb_{0.85}La_{0.15}TiO_3$ (PLT15) ferroelectric ceramic samples. The samples were prepared with average grain size of 1.69 ± 0.08 μm and 146 ± 8 nm using, respectively, conventional and spark plasma sintering techniques. A decrease in the tetragonality degree as the crystallite size decreased was explained by an internal stress caused by the existence of a large amount of grain boundaries. The local structure exhibited no significant modification and the dielectric measurements showed a diffuse phase transition and a reduction in the permittivity magnitude at T_m as the average grain size decreased. The nanostructured ceramic sample prepared at a relatively lower temperature and sintering time presented a dielectric constant value of approximately 2000 at room temperature.

Keywords: B. Grain size; Ferroelectrics; PLT; Spark plasma; Raman; XANES

1. Introduction

Lead titanate, $PbTiO_3$ (PT), is a well-known perovskite-type ferroelectric ceramic characterized by remarkable ferroelectric, piezoelectric and pyroelectric properties [1]. However, it exhibits a structure with a large degree of tetragonality (c/a), i.e., 1.064, resulting in a large stress within the lattice, which hampers the preparation of pure and dense PT ceramics [2]. La^{3+} has been widely used as a dopant to prepare dense PT solid solutions, and the isomorphic substitution of Pb^{2+} ions by La^{3+} ions has improved its mechanical and ferroelectric characteristics [3–5]. Lead lanthanum titanate, $Pb_{1-x}La_xTiO_3$ (PLT), displays a decrease in both Curie temperature and tetragonality degree as the amount of La increases and the relaxor ferroelectric behavior has been identified in compositions containing more than 24 at.% of lanthanum [1]. These properties have made the PLT system an interesting candidate for technological applications as pyroelectric, piezoelectric or electro-optic devices, optical waveguides, infrared sensors, dynamic random access memories and non-volatile memories [3,4,6,7].

In the last decades, several processing methods to synthesize materials on a nanometer scale have been developed and the study of these nanostructured materials revealed novel properties which cannot be expected for conventional microcrystalline materials [8]. The influence of grain size on the properties of ferroelectric materials has drawn plenty of attention and several studies have been conducted because of their potential technological applications [9]. These studies revealed two critical sizes that exert a major influence on ferroelectricity [10]; one, occurs in the submicron size range and is characterized by a transition from multi-domain to single-domain grains and has been found to be about 300 nm in $PbZr_{0.95}Ti_{0.05}O_3$ crystallites [10]. The second one, involves the disappearance of ferroelectric behavior and studies have reported a critical size as 30 nm for $BaTiO_3$ powder particles and 7–14 nm for $PbTiO_3$ thin films [10].

* Corresponding author. Tel.: +55 1633739828; fax: +55 1633739824.
E-mail addresses: lexmesquita@gmail.com (A. Mesquita), valmor@ifsc.usp.br (V.R. Mastelaro).

0272-8842/$36.00
http://dx.doi.org/10.1016/j.ceramint.2012.04.039

Nevertheless, most of the studies on the size influence on nanostructured ferroelectric materials have involved the preparation of thin films and relatively simple ceramic compositions, as $BaTiO_3$ [10,11]. It is well known that the characteristics (purity, size, morphology) of the powder used in the synthesis of dense ceramic samples are crucial to obtain samples with improved properties. Moreover, the use of nanostructured powders has contributed to the sintering process. Plenty of attention has been devoted to the development of new synthesis processes for the densification of nanocrystalline ceramics and, recently, some studies have described the influence of particle size on the ferroelectric properties of ceramic samples [12–14].

Buscaglia et al. [12] studied dense $BaTiO_3$ nanostructured ceramics varying their average grain size by a spark plasma sintering technique (SPS). Based on dielectric measurements, they showed that the dielectric phase transition progressively assumed a more diffuse character as the particle size decreased [12]. Moreover, a shift in the Curie temperature by decreasing the grain size towards lower values was observed, mainly when the grain size was smaller than 100 nm [12]. Jiang et al. observed a similar behavior when they studied $PbTiO_3$ nanocrystalline ceramics [13].

It has also been shown that the ferroelectric character changes as the average grain decreases [14,15]. Carreaud et al. [14] observed a decrease in the dielectric maximum resulting in the disappearance of the relaxor state with no change of diffusivity. It is important to note that in this case, they studied ceramic samples with a lower density (around 60%). Algueró et al. [15] observed an evolution from micron-sized lamellar domains towards submicron/nanometer sized crosshatched domains in function of average grain size decrease, resulting in a sample with a certain degree of electrical relaxor behavior.

In the lead-based ferroelectric compounds, the relationship between the local order structure and the ferroelectric properties has been studied in details [16,17]. However, at the best of our knowledge, the effect of grain size on the short-range order structure and thus on their ferroelectric properties, mainly for complex perovskite ferroelectric ceramic compounds, is not well established.

As the ferroelectric properties have shown to be dependent on the material structure on different scales, the aim of the present study is to provide an analysis of the effect of particle size on the short and long-range order structure and the dielectric behavior of $Pb_{0.85}La_{0.15}TiO_3$ (PLT15) ferroelectric ceramic samples. This composition was chosen because it presents a classic ferroelectric behavior for micrometric grain sizes [1]. Samples of different particle sizes were prepared by the polymeric precursor method modifying their annealing temperature, and their structural, microstructural and dielectric properties were investigated. SPS technique and conventional sintering method were respectively used to prepare dense nano- and micro-crystallized ceramic samples using nanocrystalline PLT15 powder sample.

2. Experimental procedure

The $Pb_{0.85}La_{0.15}TiO_3$ (PLT15) nanocrystalline powder was prepared by the polymeric precursor method, also referred to as the Pechini method [18]. The details of this preparation, which can be found elsewhere, involve the formation of a polymeric network followed by a heat-treatment at 400 °C for 4 h to eliminate the organic precursors [19]. After this heat treatment, PLT15 nanopowder was annealed at temperatures of 500, 600, 700, 800, 900 and 1000 °C for 2 h. PLT15 samples were labeled as PLT15x, where x represents the annealing temperature in Celsius degrees.

The microstructural characterization was carried out in a high resolution scanning electron microscope (FE-SEM Supra 35, Zeiss, Germany) operating at 3 kV. The grain size distribution was determined for each sample and then fitted using a Gaussian distribution function.

The X-ray powder diffraction (XRD) patterns were measured at room temperature on a Rigaku Denki powder diffractometer with θ–2θ geometry, a rotating anode X-ray source (Cu-K_α radiation, $\lambda = 1.542$ Å), and a scintillation detector. The measurements were taken using 100 mA current and 50 kV tension. The data were collected at a step size of 0.02° and a count time of 5 s per step. The structure was refined by the Rietveld method [20] using FullProf program [21].

Raman scattering measurements were performed using a Coherent INNOVA 70C Spectrum laser and a Jobin-Yvon T64000 triple monochromator with a charge coupled device detector. The 514 nm line of an argon laser was used as the exciting light, with the power kept below 1 mW.

The titanium K-edge X-ray absorption spectra were collected at the LNLS (National Synchrotron Light Laboratory, Campinas, Brazil) facility using a D04B-XAS1 beamline. The LNLS storage ring was operated at 1.36 GeV and 100–160 mA. The sample pellets, obtained after sintering, were grounded for X-ray absorption spectroscopy (XAS) measurements. XAS data were collected at Ti K-edge (4966 eV) in transmission mode at room temperature using a Si(1 1 1) channel-cut monochromator. Ionization chambers were used to detect the incident and transmitted flux. The X-ray absorption near edge spectroscopy (XANES) at the Ti K-edge were collected between 4910 and 5200 eV using energy steps of 0.5 eV. To provide good energy reproducibility during the XANES data collection, the energy calibration of the monochromator was checked using a Ti metal foil. Normalized XANES spectra were obtained by the Multiplatform Applications for XAFS code (MAX) [22].

PLT15700 nanocrystalline powder was sintered by SPS technique using DR SINTEX Lab 515SA equipment. Firstly, the powder was placed in an SPS graphite die and an electric current of approximately 500 A was applied under a pressure of 49.7 MPa. After 7 min, the temperature was raised to 950 °C and kept constant for 10 min. Then, the current was switched off, the pressure was released and the temperature of the sample was cooled to room temperature. The resulting pellets were annealed in air at 900 °C for 2 h in order to relieve the residual stresses, remove the surface carbon contamination, and eliminate the oxygen vacancies possibly produced during the SPS synthesis [23]. The PLT15700 powder sample was also sintered using a conventional electric furnace at 1230 °C for 2 h in a Pb-rich atmosphere to avoid

losses in the stoichiometry. The densities of the sintered samples determined using the Archimedes method were approximately 96% for the SPS sample (PLT15_SPS) and 98% for the conventionally prepared sample (PLT15_CS). The complex dielectric permittivity of both samples was measured from room temperature up to 500 °C using an impedance/gain-phase analyzer (Solartron SI 1260) operating from 1 kHz to 1 MHz.

3. Results and discussion

Fig. 1(a) shows the FE-SEM image of the PLT15 powder sample calcined at 700 °C for 2 h (PLT15700) which presents an average particle size of 43 ± 5 nm and a significant particle coalescence process. Fig. 1(b) and (c) depict, respectively, the images of the samples annealed at 900 (PLT15900) and 1000 °C (PLT151000). The grains present an average sizes of

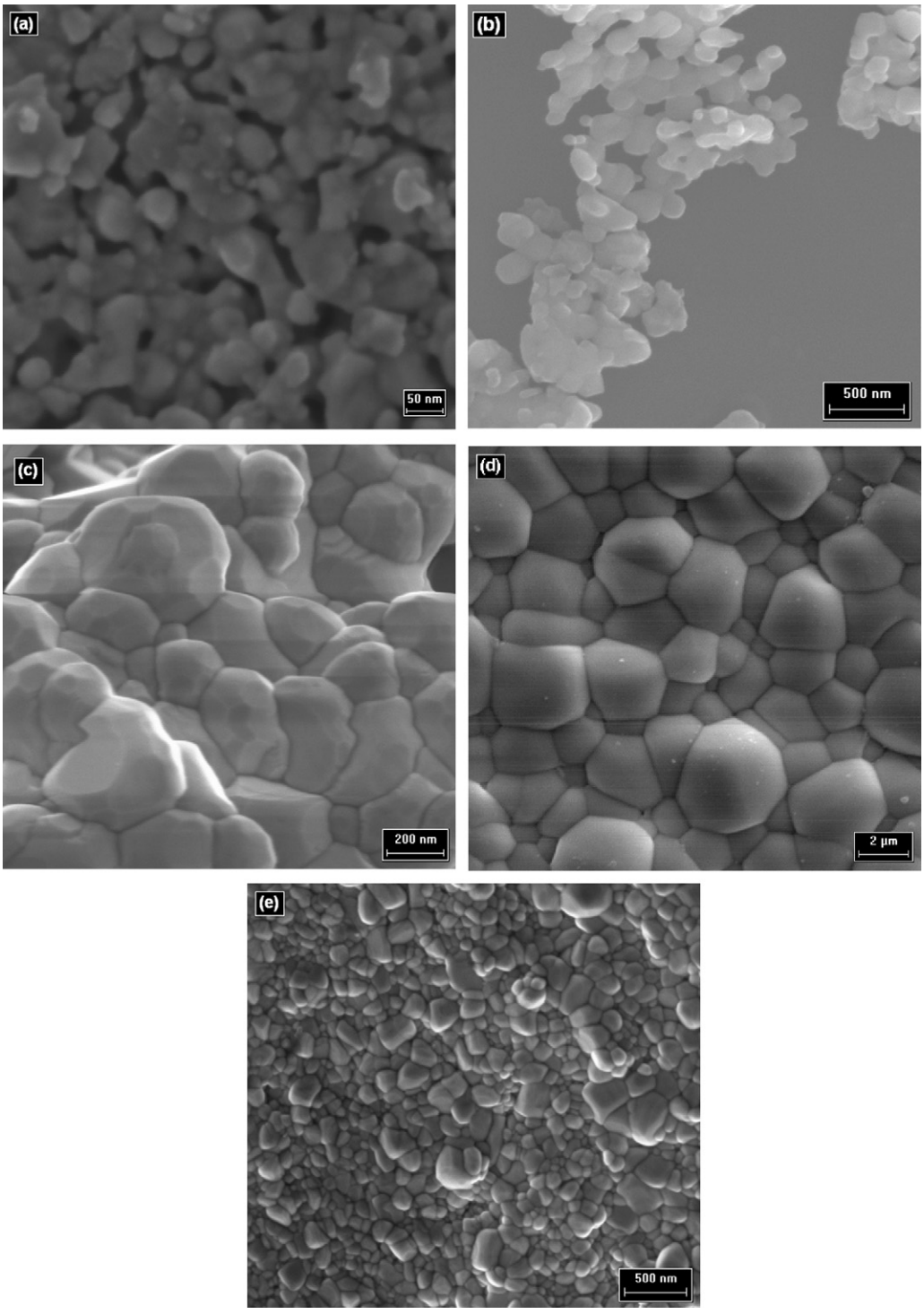

Fig. 1. Scanning electron microscopy for PLT15 samples annealed at (a) 700, (b) 900 and (c) 1000 and samples sintered (d) conventionally and (e) by SPS technique.

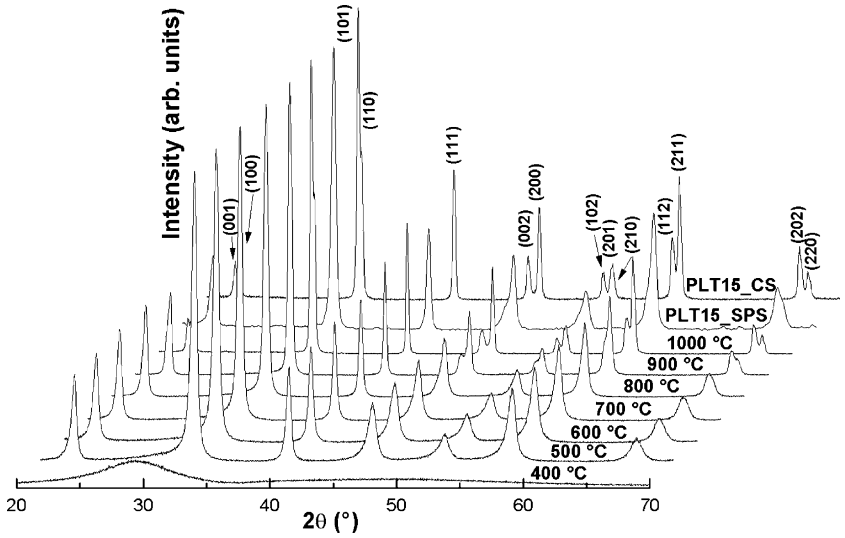

Fig. 2. XRD patterns for PLT15 samples annealed at different temperatures and for the ceramic samples sintered conventionally and by SPS technique.

157 ± 7 nm for PLT15900 and 191 ± 10 nm for PLT151000. The analyses of the micrographs suggest that larger particles can be formed by a single particle or by an agglomeration process of smaller particles.

The average grain sizes determined from the analysis of the SEM images of PLT15_CS and PLT15_SPS samples (Fig. 1(d) and (e)) were 1.69 ± 0.08 μm and 146 ± 8 nm, respectively. As expected, high temperature and sintering time favor the grain growth leading to micrometric grain sizes for the PLT15_CS sample. The analysis of the average grain sizes shows that PLT15 calcined samples presents an almost linear growth rate as a function of annealing temperature up to 1000 °C. The growth rate of PLT15_CS sintered sample does not follow this behavior because the mechanism of growth in this case involves at least two stages [24]. The first stage includes the removal of internal stress and the interface structure relaxation at lower temperature and the second is mainly the growth of grains at high temperatures which is related to sintering process [24].

Fig. 2 shows the X-ray diffraction patterns collected at room temperature as a function of the annealing temperature. In order to compare the nanocrystalline sample with the microcrystalline one, the XRD of the PLT15_CS sample is also shown. The samples crystallized completely without the presence of secondary phases and the non-calcinated PLT15 sample exhibited a diffratogram characteristic of an amorphous phase. This finding is consistent with our previous study, which demonstrate that the crystallization process occurred between 400 and 500 °C [19].

In good agreement with the literature, the diffraction planes of PLT15 samples heat-treated at relative higher temperatures correspond to a tetragonal structure with *P*4*mm* space group [25]. A decrease in the annealing temperature leads to the broadening and overlapping of the diffraction peaks, mainly those related to (0 0 1), (1 0 0), (0 0 2) and (2 0 0) diffraction planes. This overlapping indicates a transition to a more symmetric phase, i.e., a structure with characteristics of a *Pm*-3*m* cubic structure.

The XRD pattern of the PLT15_SPS sample is also shown in Fig. 2. No secondary phase is observed and the overlapping of (0 0 2) and (2 0 0) planes indicates a lower tetragonality degree compared to PLT15_1000 and PLT15_CS samples.

A Rietveld refinement was carried out using a tetragonal structure with *P*4*mm* space group as the initial model. The

Table 1
Cell parameters and data statistics calculated from Rietveld method and crystallite size for PLT15 samples.

Annealing temperature (°C)	*a* (nm)	*c* (nm)	R_{Bragg}	χ^2	Crystallite size (nm)
500	0.3938(2)	0.3989(3)	4.85	15.1	19
600	0.3937(1)	0.3983(6)	3.39	14.1	23
700	0.3934(9)	0.3979(2)	3.25	11.4	26
800	0.3930(7)	0.3972(2)	3.55	13.1	35
900	0.3927(3)	0.3976(9)	2.71	9.8	90
1000	0.3935(2)	0.3975(2)	1.02	13.8	117
700[a]	0.3924(3)	0.3971(7)	5.31	12.8	103
1230[b]	0.3921(6)	0.3992(5)	2.25	2.4	203
500[c]	0.3962(7)	–	13.46	21.70	–
700[c]	0.3950(4)	–	11.70	22.71	–

[a] Sintering temperature by SPS.
[b] Sintering temperature by CS.
[c] Refined as a cubic structure.

lattice parameters calculated in the refinement and the R_{Bragg} and χ^2 quality factors are shown in Table 1. A cubic model with *Pm*-3*m* space group was also used as the initial model in the Rietveld refinements for PLT15500 and PLT15700 samples. However, the refinements data did not converge well and the quality factors were worse than those of the refinements when a tetragonal model was used. Thus, PLT15 samples annealed at lower temperatures also showed a tetragonal structure with a *P*4*mm* space group.

Table 1 shows the crystallite size values of all samples evaluated using Scherrer's equation [26]. The average crystallite size was calculated using the full width at half maximum of (1 1 1) peaks from the XRD patterns for all samples depicted in Fig. 2. The average crystallite size is much smaller than the average grain size evaluated through the SEM measurements, meaning that each particle consists of several coherent diffracting domains, which is in agreement with a previous study [27].

Fig. 3 shows the Raman spectra for PLT15 samples annealed at 400, 600, 700, 800, 900 °C and for PLT15_CS and PLT15_SPS samples. The modes were identified according to the vibrational modes of pure $PbTiO_3$ [28]. A_1(1TO) and E(1TO) soft modes are the lower frequency modes and can provide important information about the symmetry of the perovskite cell. In E(1TO), both Ti and O ions move in the opposite direction of the Pb displacement in [1 0 0] or [0 1 0] directions. The A_1(1TO) corresponds to a similar movement in the [0 0 1] direction. Thus, the displacement occurs in the direction of the lattice parameter *a* for E(1TO) and in the direction of the lattice parameter *c* for A_1(1TO), indicating a structural phase transition [28].

In good agreement with the XRD data, the Raman spectrum of PLT15400 samples is typical of amorphous materials. The samples annealed at higher temperatures show a shift in the frequency of E(1TO) and A_1(1TO) soft modes when compared to the spectra of sintered samples. Moreover, the intensity of these modes increases and the full width at half maximum of the

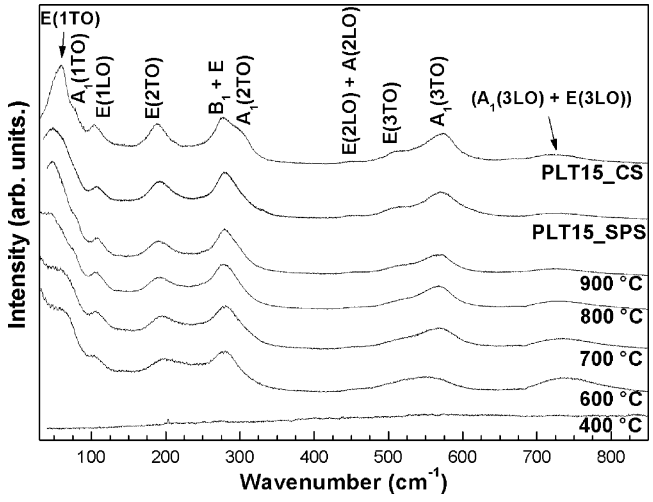

Fig. 3. Raman spectra for PLT15 samples annealed at 400, 600, 700, 800, 900 °C and for the ceramic samples sintered conventionally and by SPS technique.

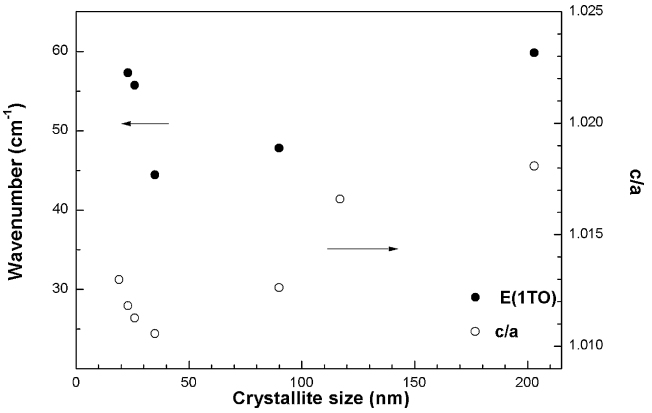

Fig. 4. E(1TO) frequency and *c*/*a* as a function of crystallite size.

Raman peaks decreases as the particle size increases. These changes in the Raman spectra have been attributed to a stress effect, which appears as domain splitting and is hindered by neighboring grains with different orientations [29]. The Raman spectra of the PLT15_SPS sample are quite similar to those of calcined samples whereas the Raman spectra of the PLT_CS sample show well-defined bands characteristic of microstructured samples and a higher degree of tetragonality.

Fig. 4 shows the dependence of the E(1TO) soft mode frequency and the tetragonality degree (*c*/*a*) as a function of the crystallite size. As can be verified, the frequency of E(1TO) mode and the *c*/*a* have a similar behavior with the increase in the crystallite size. First, both parameters decrease as the crystallite size grows from 19 nm to 35 nm. Then they increase as the crystallite size exhibits a micrometer scale. As previously discussed, the frequency decrease of the E(1TO) soft mode is related to a phase transition, therefore this mode and the *c*/*a* values are expected to present a similar behavior.

The *c*/*a* value of the PLT15_CS sample is equal to 1.018, in agreement with previous studies of PLT15 sample prepared by the solid state reaction method [1,30]. The decrease in the *c*/*a* value up to 1.010 when the grain size is equal to 35 nm was attributed to the existence of an internal stress in each crystallite which depends on the orientation of all surrounding crystallites [27]. This stress consists of a combination of uniform mechanical compression along the *c* axis and tensions along the *a* axes leading to a decrease in the tetragonality degree [27]. As the crystallite size decreases from 35 to 19 nm, the *c*/*a* value increases to 1.013.

A similar behavior was also reported by Mandal et al. in a study of the particle size of $PbZr_{0.70}Ti_{0.30}O_3$ sample prepared by a polymeric precursor method [31]. According to the authors, the decrease in the particle size would induce an increase in the surface area of the particles, therefore, inducing modifications in the symmetry of the octahedral BO_6 units occasioned by a large number of Zr^{4+} and Ti^{4+} on the surface structure [31].

In order to investigate the effect of particle size on the local order structure around Ti atom, Ti K-edge XANES spectra were measured. As observed in Fig. 5, the short and medium-range order structures around Ti atoms are not affected by the decrease of the particle size. The difference in pre-edge peaks

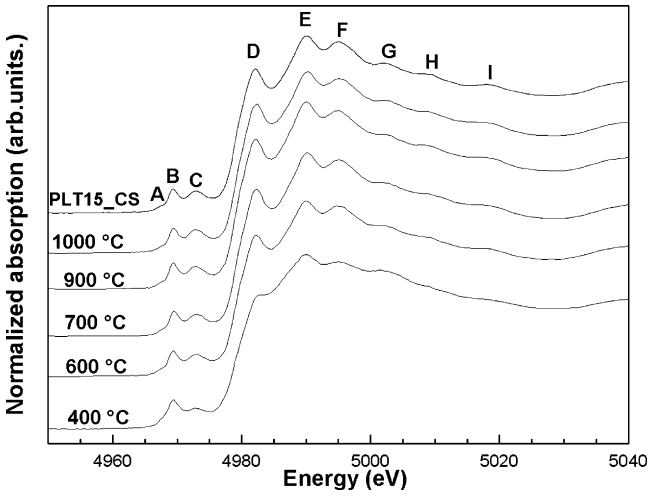

Fig. 5. XANES spectra at Ti K-edge for PLT15 samples.

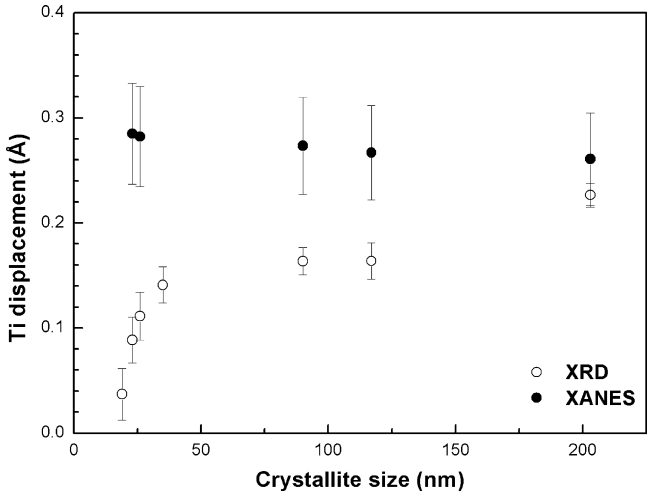

Fig. 6. Static Ti displacement evaluated by XANES and XRD measurements for PLT15 samples.

of the PLT15400 sample is attributed to a higher local disorder around Ti atoms, as this sample is in an amorphous state.

The pre-edge region of K-edge XANES spectra of some transition metal oxides is characterized by some features several volts before the absorption edge [16]. In transition metal oxides that crystallize in centrosymmetric structures, the intensity of these pre-edge features is very small or even absent, however, in non-centrosymmetric structures it can be relatively large [16]. According to Vedrinskii et al., the physical origin of the pre-edge feature labeled as *A* is related to quadrupolar transitions of t_{2g}-type molecular orbitals located in the absorption atom [16]. The authors also show that the transition named *B* is caused by the hybridization of *p*- and *d*-symmetry states at the Ti atom under the influence of the neighboring oxygen atoms [16]. Moreover, the high intensity of this transition is a qualitative indication of ferroelectricity in the perovskite structure and can be successfully used to determine the mean-square (static or dynamic) displacements of Ti atoms from the center of coordination octahedra [16].

The pre-edge feature labeled *C* in Fig. 5 is related to the Ti 1*s* electron transition to the unoccupied 3*d*-originated e_g-type molecular orbital of TiO_6 polyhedra neighboring the absorbing Ti atoms, which are weakly affected by the core hole potential [16]. The area of the *C* peak does not depend strongly on small displacements of the atoms from their sites in cubic crystal lattice, but it changes significantly when 4*d* atoms, as Zr in PZT solid solution appear in the vicinity of the absorbing Ti atom [16]. The transitions labeled *D*, *E*, *F*, *G*, *H* and *I* beyond the absorption edge are related to electronic transitions and the atomic structure of the second and third neighbors of the Ti atom in a distance up to 8 Å from this atom [1,32].

The displacement of Ti atoms from their centrosymmetric position on the TiO_6 octahedra can be determined by the calculation of the area under the *B* peak using a Lorentz function [33]. Fig. 6 shows the displacement of the Ti atom in comparison with the displacement calculated from XRD data [33]. No variation of the Ti displacement value evaluated from XANES measurements is observed within the experimental error as the crystallite size rises. However, the displacement of Ti atoms obtained from the Rietveld refinement results decreases as the crystallite size decreases towards the centrosymmetric position for Ti atoms in a perovskite unit cell. In other words, XRD data show that the magnitude of the Ti off-center position decreases as the crystallite size diminishes, reaching an idealized cubic perovskite structure. Thus, XANES and XRD measurements provide different values of the Ti off-center position as a function of the crystallite size. This difference is basically due to the fact that X-ray absorption spectroscopy (XAS) probed the short-range order around Ti atoms whereas XRD provides structural information about the local average structure [1].

Guinier's classic crystallography textbook [34] explains clearly why Bragg peaks intensities and profiles contain only long-range order information, and why diffraction information on local disorder is located in the diffuse scattering, which is not included in standard refinement procedures, and much difficult to interpret quantitatively. This is why Rietveld refinement of disordered crystals powder diffraction patterns, which assumes by principle a long-range crystallographic order, leads systematically to an average crystal structure, ignoring local distortions if they are randomly distributed in the material. The ability to complete XRD studies by local structural probes, such as XAS refinements has been discovered and published on alloys and inorganic materials such as solid solutions since the early eighties [35–40]. In most cases local probes evidenced local relaxation of the crystal lattice, which was impossible to observe in the long-range order crystal structures.

Concerning the perovskite titanates materials, the difference concerning the local symmetry detected by XRD and XAS techniques was first observed by Sicron et al. when they compared the local symmetry around Pb and Ti atoms on the paraelectric phase of $PbTiO_3$ compound [17]. They attributed this difference in terms of the disorder level that these techniques can detect. In their samples, they interpreted this disorder to orientation disorder of the Ti off-center axis, leading to an XRD average regular TiO_6 octahedron, whereas XAS can

detect this local distortion even while it is not crystallographically oriented. In X-ray absorption spectroscopy, the physical process involved in the absorption occurs in the order of 10^{-16} s [17]. This time is less than the time scale of the changes in the system, enabling to observe dynamic and fast disorder processes [17]. Summarizing, the discrepancy is basically due to the fact that X-ray absorption spectroscopy probed the short-range order, whereas in X-ray diffraction the used models that provides structural information about the average structure where the local disorder is not considered [1].

The dielectric permittivity of nano and microstructured ceramic sintered samples as a function of the temperature was measured at 1 kHz, 10 kHz, 100 kHz and 1 MHz. Real (ε') and imaginary (ε'') parts and the corresponding curves of PLT15_CS and PLT15_SPS samples are shown in Fig. 7. Regarding the PLT15_CS sample (Fig. 7(a)), as expected, the dielectric measurements did not show a frequency dispersion at the maximum temperature of the dielectric curve (T_m = 214 °C at 1 MHz) allowing characterizing this sample as a classic ferroelectric material. At higher temperatures, a dispersion in the permittivity curves is observed in real and imaginary parts.

Compared to the PLT15_CS sample, the dielectric curves of the PLT15_SPS sample are largely broadened indicating a higher degree of diffuseness in the dielectric behavior at phase transition. However, no significant shift of T_m with the increase in frequency is observed, which allows identifying a relaxor-like dielectric character. Our results clearly show that in the case of nanostructured ceramic PLT15_SPS sample, even with the sample presenting a nanometric grain size, the polar long-range order persists and the domain structure is characteristic of a normal ferroelectric compound with a diffuse phase transition. A similar behavior was also observed for $BaTiO_3$ compound, as the grain size decreased [12]. According to Buscaglia et al. [12], as the local tetragonality changes due to the grain size distribution, different Curie temperatures are expected locally and as a result, a very broad dielectric curve is observed in nanocrystalline ceramics.

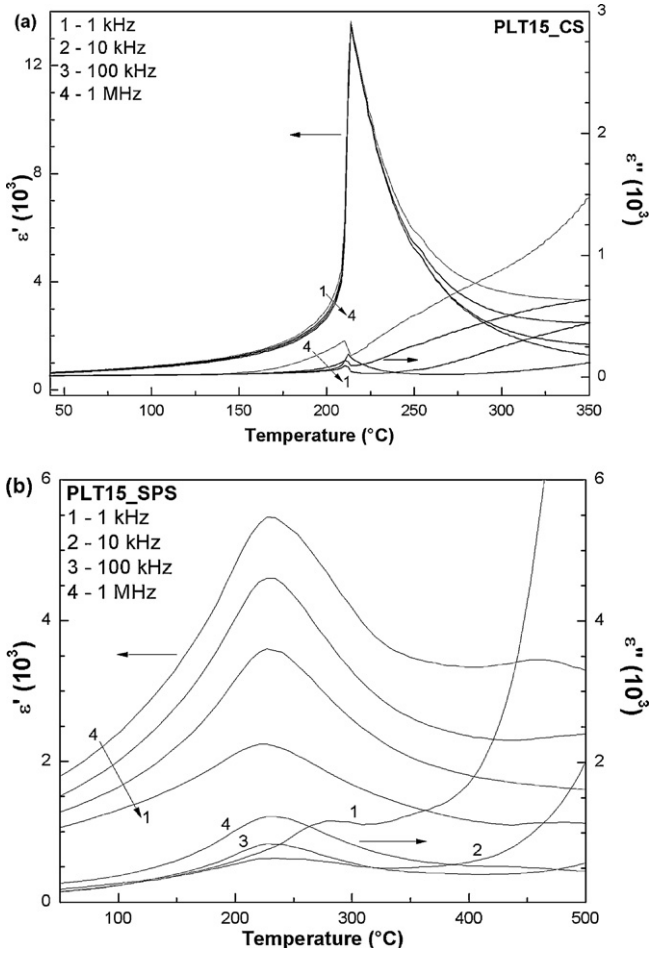

Fig. 7. Dielectric permittivity as a function of the temperature for (a) PLT15_CS and (b) PLT15_SPS.

A decrease was also verified in the magnitude of the maximum of dielectric permittivity of the PLT15_SPS sample compared with the PLT15_CS one. As the grain size decreases, the magnitude of the dielectric permittivity is gradually depressed due to the dilution effect exerted by the increasing number of non-ferroelectric grain boundaries [12]. Although the decrease in the grain size leads to a reduction from approximately 12,000 to 5000 in the magnitude of the dielectric permittivity (ε') at T_C, near room temperature, the nanostructured sample presents a relatively higher dielectric permittivity value, i.e., 2000. As pointed out in the literature, in the case of nanostructured thin films, biaxial strain effects can be used to enhance the tetragonal ordering, hence the remanent polarization [41,42]. In the case of nanostructured ceramics, a solution to restore the permittivity dielectric magnitude is still a challenge [42]. The dielectric anomaly observed mainly in the high temperature range of the dielectric permittivity curve of the nanocrystalline PLT15_SPS sample has been also detected in different microstructured ferroelectric perovskite compounds [43,44]. According to Kang et al. [36], such an anomaly is an extrinsic phenomenon and should be observed in all perovskite oxides regardless of the processing parameters or the composition because oxygen vacancies can be thermally formed as the temperature increases. M'Peko et al. showed that the large dielectric anomaly associated with an abrupt permittivity rise in ferroelectric ceramic materials is related to a low-frequency dielectric dispersion phenomenon due to polarization from charge storage processes at the grain boundaries [45]. In these regions, which are more resistive, the electrical charges move slowly resulting in an interfacial polarization mechanism [45].

4. Conclusions

The structural and dielectric properties of dense nanostructured and microstructured $Pb_{0.85}La_{0.15}TiO_3$ ferroelectric ceramic samples have been characterized. The XRD results showed a reduction in the degree of tetragonality in the nanostructured ceramic sample whereas XAS and Raman techniques showed that the local order is less affected by the grain size reduction.

The decrease in the average grain size to a nanometer scale induced a diffuse phase transition and a reduction in the permittivity magnitude at T_m. The reduction in the magnitude

of the dielectric permittivity of nanostructured samples compared to microstructured samples was related to the difference between the core grain and the grain boundaries which, in nanocrystalline samples, are non-ferroelectric regions. The diffuse phase transition behavior was explained in terms of the existence of various distributed Curie temperatures due to the local tetragonality changes related to the grain size distribution. Although a decrease was observed in the magnitude of the dielectric permittivity as the grain size was reduced, the synthesis methodology used in this work has shown that with nanosized particles it is possible to obtain compact ceramic samples with a relatively high dielectric constant at lower temperatures and time of sintering. These ceramics can be useful when it is necessary to reduce their size for use in miniaturized systems.

Acknowledgements

The authors would like to acknowledge R. Camargo (DQ–UFSCar, Brazil) for the SEM measurements. This research was partially developed at LNLS – National Laboratory of Synchrotron Light, Brazil and was supported by FAPESP and CNPq Brazilian agencies.

References

[1] P.P. Neves, A.C. Doriguetto, V.R. Mastelaro, L.P. Lopes, Y.P. Mascarenhas, A. Michalowicz, J.A. Eiras, XAS and XRD structural characterization of lanthanum-modified $PbTiO_3$ ceramic materials, Journal of Physical Chemistry B 108 (2004) 14840–14849.

[2] H. Wang, L. Wang, J.B. Liu, B. Wang, H. Yan, Preparation of $Pb_{1-x}La_xTi_{1-x/4}O_3$ ($x = 0.28$) powders by a sol–gel–hydrothermal method, Materials Science & Engineering B-Solid 99 (2003) 495–498.

[3] S. Murakami, M. Herren, D. Rau, T. Sakurai, M. Morita, Low-temperature luminescence and energy transfer processes in Eu^{3+}, Nd^{3+}, and Cr-doped sol–gel PLZT ceramics, Journal of Luminescence 83/4 (1999) 215–219.

[4] A.K. Arora, R.P. Tandon, A. Mansingh, Piezoelectric, pyroelectric and dielectric properties of lanthanum modified lead zirconate titanate ceramics, Ferroelectrics 132 (1992) 9–25.

[5] A. Sternberg, Recent advances in transparent ferroelectric ceramics research and applications, Ferroelectrics 134 (1992) 29–34.

[6] J.H.G. Rangel, P.R.G. Goncalves, M.M. Oliveira, M.I.B. Bernardi, E. Longo, L.E.B. Soledade, I.M.G. Santos, A.G. Souza, Nanometric $Pb_{1-x}La_xTiO_3$ ($x = 0$, 0.13 and 0.27) powders obtained by the polymeric precursor method, Materials Research Bulletin 43 (2008) 825–835.

[7] V.R. Mastelaro, P.P. Neves, S.R. de Lazaro, E. Longo, A. Michalowicz, J.A. Eiras, Electronic structure of $Pb_{1-x}La_xTiO_3$ ferroelectric materials from Ti 2p and O 1s soft X-ray absorption spectroscopy, Journal of Applied Physiology 99 (2006).

[8] T. Watanabe, S. Tsurekawa, Preface to the special issue on grain boundary engineering, Journal of Materials Science 40 (2005) 817.

[9] E.K. Akdogan, C.J. Rawn, W.D. Porter, E.A. Payzant, A. Safari, Size effects in $PbTiO_3$ nanocrystals: effect of particle size on spontaneous polarization and strains, Journal of Applied Physics 97 (2005).

[10] S. Berger, Size effect on ferroelectric behavior, Transactions of the Indian Institute of Metals 58 (2005) 1141–1156.

[11] C. Ziebert, H. Schmitt, J.K. Kruger, A. Sternberg, K.H. Ehses, Grain-size-induced relaxor properties in nanocrystalline perovskite films, Physical Review B 69 (2004) 214106.

[12] V. Buscaglia, M.T. Buscaglia, M. Viviani, L. Mitoseriu, P. Nanni, V. Trefiletti, P. Piaggio, I. Gregora, T. Ostapchuk, J. Pokorny, J. Petzelt, Grain size and grain boundary-related effects on the properties of nanocrystalline barium titanate ceramics, Journal of the European Ceramic Society 26 (2006) 2889–2898.

[13] Q. Jiang, X.F. Cui, M. Zhao, Size effects on Curie temperature of ferroelectric particles, Applied Physics A-Materials Science & Processing 78 (2004) 703–704.

[14] J. Carreaud, P. Gemeiner, J.M. Kiat, B. Dkhil, C. Bogicevic, T. Rojac, B. Malic, Size-driven relaxation and polar states in $PbMg_{1/3}Nb_{2/3}O_3$-based system, Physical Review B 72 (2005) 174115.

[15] M. Alguero, J. Ricote, R. Jimenez, P. Ramos, J. Carreaud, B. Dkhil, Size effect in morphotropic phase boundary $Pb(Mg_{1/3}Nb_{2/3})O$-3-$PbTiO_3$, Applied Physics Letters 91 (2007) 3.

[16] R.V. Vedrinskii, V.L. Kraizman, A.A. Novakovich, P.V. Demekhin, S.V. Urazhdin, Pre-edge fine structure of the 3d atom K X-ray absorption spectra and quantitative atomic structure determinations for ferroelectric perovskite structure crystals, Journal of Physics-Condensed Matter 10 (1998) 9561–9580.

[17] N. Sicron, B. Ravel, Y. Yacoby, E.A. Stern, F. Dogan, J.J. Rehr, Nature of the ferroelectric phase transition in $PbTiO_3$, Physical Review B 50 (1994) 13168–13180.

[18] M.P. Pechini, Method of preparing lead and alkaline – earth titanates and niobates and coatings method using the same to form a capacitor in: U.S. Patent, 1967.

[19] A. Mesquita, M.I.B. Bernardi, L.J.Q. Maia, V.R. Mastelaro, Synthesis and characterization of $Pb_{1-x}La_xTiO_3$ nanocrystalline powders, Journal of Thermal Analysis and Calorimetry 87 (2007) 747–751.

[20] H.M. Rietveld, A profile refinement method for nuclear and magnetic structures, Journal of Applied Crystallography 2 (1969) 65–71.

[21] J. Rodríguez-Carvajal, Abstracts of Satellite Meeting on Powder Diffraction of the XV Congress of the IUCr, 2005, p. 127.

[22] A. Michalowicz, J. Moscovici, D. Muller-Bouvet, K. Provost, MAX multiplatform applications for XAFS, Journal of Physics: Conference Series 190 (2009) 012034.

[23] M.T. Buscaglia, M. Viviani, Z. Zhao, V. Buscaglia, P. Nanni, Synthesis of $BaTiO_3$ core–shell particles and fabrication of dielectric ceramics with local graded structure, Chemistry of Materials 18 (2006) 4002–4010.

[24] Q.F. Zhou, H.L.W. Chan, Q.Q. Zhang, C.L. Choy, Raman spectra and structural phase transition in nanocrystalline lead lanthanum titanate, Journal of Applied Physics 89 (2001) 8121–8126.

[25] O. Yamaguchi, A. Narai, T. Komatsu, K. Shimizu, Crystallization and transformation of distorted cubic $PbTiO_3$, Journal of the American Ceramic Society 69 (1986) C256–C257.

[26] M.P. Klug, L.E. Alexander, X-ray Diffraction Procedure for Polycrystalline and Amorphous Materials, Wiley-Interscience Publication, New York, 1974.

[27] S. Chattopadhyay, P. Ayyub, V.R. Palkar, M. Multani, Size-induced diffuse phase-transition in the nanocrystalline ferroelectric $PbTiO_3$, Physical Review B 52 (1995) 13177–13183.

[28] J.D. Freire, R.S. Katiyar, Lattice-dynamics of crystals with tetragonal $BaTiO_3$ structure, Physical Review B 37 (1988) 2074–2085.

[29] D. Wu, A.D. Li, C.Z. Ge, P. Lu, C.Y. Xu, J. Xu, N.B. Ming, Raman spectroscopy and X-ray diffraction study of sol–gel derived $(PB_{1-x}La_x)Ti_{1-x/4}O_3$ thin films on Si substrates, Thin Solid Films 322 (1998) 323–328.

[30] E.C.S. Tavares, P.S. Pizani, J.A. Eiras, Short-range disorder in lanthanum-doped lead titanate ceramics probed by Raman scattering, Applied Physics Letters 72 (1998) 897–899.

[31] T.K. Mandal, S. Ram, Synthesis of $PbZr_{0.7}Ti_{0.3}O_3$ nanoparticles in a new tetragonal crystal structure with a polymer precursor, Materials Letters 57 (2003) 2432–2442.

[32] V.R. Mastelaro, A. Mesquita, P.P. Neves, A. Michalowicz, M. Bounif, P.S. Pizani, M.R. Joya, J.A. Eiras, Short-range structure of $Pb_{1-x}Ba_x Zr_{0.65}Ti_{0.35}O_3$ ceramic compounds probed by XAS and Raman scattering techniques, Journal of Applied Physics 105 (2009) 033508.

[33] A.I. Frenkel, D.M. Pease, J. Giniewicz, E.A. Stern, D.L. Brewe, M. Daniel, J. Budnick, Concentration-dependent short-range order in the relaxor ferroelectric $(1 - x)$Pb(Sc,Ta)O-3-xPbTiO(3), Physical Review B 70 (2004).

[34] A. Guinier, X-ray Diffraction in Crystals and Imperfect Crystals and Amorphous Bodies, Dover Publications, New York, 1995.
[35] Y. Mathey, A. Michalowicz, P. Toffoli, G. Vlaic, Resolution of a structural disorder through apparently inconsistent X-ray diffraction and EXAFS data: structure of the new layered system manganese copper phosphorus sulfide ($Mn_{1-x}Cu_{2x}$)PS_3 ($x = 0.13$), Inorganic Chemistry 23 (1984) 897–902.
[36] Y. Mathey, H. Mercier, A. Michalowicz, A. Leblanc, Metal vacancies and partial disorder in the layers of $Cu_{0.5}Cr_{0.5}Ps_3$—an EXAFS reinvestigation of the structure, Journal of Physics and Chemistry of Solids 46 (1985) 1025–1029.
[37] A. Michalowicz, M. Verdaguer, Y. Mathey, R. Clement, Order and disorder in low dimensional materials—beyond the 1st coordination sphere with EXAFS, Topics in Current Chemistry 145 (1988) 107–149.
[38] J.C. Mikkelsen, J.B. Boyce, Atomic-scale structure of random solid solutions: extended X-ray-absorption fine-structure study of $Ga_{1-x}In_xAs$, Physical Review Letters 49 (1982) 1412–1415.
[39] A. Kuzmin, N. Mironova, J. Purans, A. Rodionov, X-ray absorption spectroscopy study of $Ni_cMg_{1-c}O$ solid solutions on the Ni K edge, Journal of Physics-Condensed Matter 7 (1995) 9357–9368.
[40] S.C. Tarantino, P. Ghigna, C. McCammon, R. Amantea, M.A. Carpenter, Local structural properties of (Mn,Fe)Nb_2O_6 from Mössbauer and X-ray absorption spectroscopy, AcCrB 61 (2005) 250–257.
[41] K.J. Choi, M. Biegalski, Y.L. Li, A. Sharan, J. Schubert, R. Uecker, P. Reiche, Y.B. Chen, X.Q. Pan, V. Gopalan, L.Q. Chen, D.G. Schlom, C.B. Eom, Enhancement of ferroelectricity in strained BaTiO(3) thin films, Science 306 (2004) 1005–1009.
[42] V. Petkov, V. Buscaglia, M.T. Buscaglia, Z. Zhao, Y. Ren, Structural coherence and ferroelectricity decay in submicron- and nano-sized perovskites, Physical Review B 78 (2008).
[43] B.S. Kang, S.K. Choi, C.H. Park, Diffuse dielectric anomaly in perovskite-type ferroelectric oxides in the temperature range of 400–700 °C, Journal of Applied Physics 94 (2003) 1904–1911.
[44] A. Mesquita, V.R. Mastelaro, A. Michalowicz, In situ X-ray diffraction studies of phase transition in $Pb_{1-x}La_xZr_{0.40}Ti_{0.60}O_3$ ferroelectric ceramics, Phase Transitions 83 (2010) 251–262.
[45] J.C. M'Peko, J. Portelles, F. Calderon, G. Rodriguez, Dielectric anomaly and low frequency dispersion in ferroelectric materials at high temperatures, Journal of Materials Science 33 (1998) 1633–1637.